Adaptive Electrical Capacitance Volume Tomography

Qussai M. Marashdeh, Fernando L. Teixeira, and Liang-Shih Fan

***Abstract*—Electrical Capacitance Volume Tomography (ECVT) has shown to be an effective low-cost and high-speed imaging technique suitable for many applications, including 3D reconstruction of multiphase flow systems. In this paper, we introduce the concept of adaptive ECVT based upon the combination of a large number of small individual sensor segments to comprise synthetic capacitance "plates" of different (and possibly noncontiguous) shapes while still satisfying a minimum plate area criterion set by a given SNR. The response from different segments is combined electronically in a reconfigurable fashion. The proposed adaptive concept paves the way for ECVT to be applicable in scenarios requiring higher resolution and dynamic imaging reconstruction.**

***Index Terms*—Capacitance sensors, electrical capacitance volume tomography, multiphase flow, non-invasive process.**

I. Introduction

ELECTRICAL CAPACITANCE volume tomography (ECVT) is a noninvasive 3D sensing technology that proved very successful for imaging and characterization of diverse multiphase (gas/fluid/solid) flow systems and industrial processes [1-3]. ECVT is a natural spinoff from the earlier 2D electrical capacitance tomography (ECT) technology [4]. The literature on ECT is vast and we will not attempt to review it here; a non-inclusive list of recent overviews can be found in [5-7]. Because both ECT and ECVT employ an interrogating field that is solution to Poisson's equation [8], they are suitable for vast range of scales. Indeed, prior applications of ECT have included domains with diameters ranging from tens of microns [9] to meters [7]. As its name suggests, ECVT retrieves volumetric images of the dielectric material distribution on a 3D domain from capacitance measurements taken on its 2D boundary. The capacitance sensors (plates) in ECVT are designed to "blanket" the imaging domain with various zones of enhanced (capacitance) sensitivity. The set of all capacitances pairs measured between the plates is sought to react differently to dielectric perturbations on each volumetric "pixel" in the imaging domain. The differences in the sensor response are used, with the aid of image reconstruction algorithms, to establish a volumetric profile (image) of the dielectric distribution [10,11]. Various challenges remain associated with such reconstruction, however. Typically, changes in the capacitance values due to perturbations in the dielectric distribution are very small [12]. As a result, plate with areas larger than a minimum area (relative to the vessel size) need to be employed, as set by a required signal-to-noise level. The resulting trade-off is that large capacitor plates decrease the number of independent measurements and hence reduce ECVT image resolution. Likewise, the limited number of capacitance plates (or independent sensor measurements) imposes an upper limit on the size (via the condition number of the ill-posed imaging reconstruction problem) of the matrix of pixels, i.e. the number of degrees of freedom in the reconstruction image. Moreover, a large plate area affects the charge density distribution from the edge to the center of each plate, which can exacerbate the ill-posedness of the ECVT reconstruction problem. From all the above, it is clear that the sensor design is a key factor in achieving higher resolution in ECVT by enabling a better control of the sensitivity map distribution. An increased number of independent measurements can also mitigate the ill-posedness of reconstruction problem. An attempt at introducing added flexibility in 2D ECT was described in a very recent work where different plate sizes were connected together to form combinations of "configurable" plates [13].

To overcome these challenges, this work introduces the concept of *adaptive* ECVT, or AECVT, whereby synthetic capacitance plates are created from the combination of (small area) plate segments along the 2D boundary of the imaging domain, each plate excited by voltage signals of possibly different amplitudes and phases [14]. AECVT enables the capture a higher number of independent capacitance measurements and allows for considerably more flexibility in the "steering" of the interrogating field (intensity) throughout different regions of the imaging domain. AECVT can also combat the ill-posedness of the inverse problem through a more precise control of the spatial variation of the electric field (i.e., the sensitivity map). The use of small plate

Mansucript submitted on September 2013, revised December 2013. This work was supported in part by the U.S. Department of Energy.

Q. M. Marashdeh is with Tech4Imaging LLC, Columbus, OH 43220 USA (e-mail: marashdeh@tech4imaging.com).

F. L. Teixeira is with the ElectroScience Laboratory and Department of Electrical and Computer Engineering , The Ohio State University, Columbus, OH 43212 USA (e-mail: teixeira.5@osu.edu).

L. S. Fan is with the Department of Chemical and Biomolecular Engineering , The Ohio State University, Columbus, OH 43210 USA (e-mail: fan@chbmeng.ohio-state.edu).

segments in AECVT further adds more flexibility for the sensor shape to fit to different duct and vessel geometries, so as to include composite and/or bent shapes such as *T*-junctions or *L*-junctions, for example.

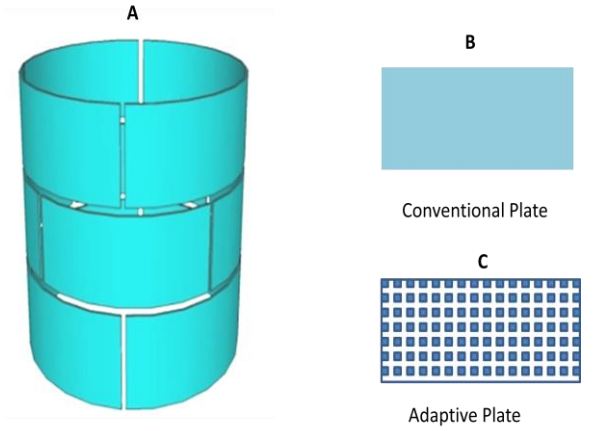

Figure 1: (a) conventional ECVT sensor with (b) conventional plate and (c) adaptive plate with segments for voltage distribution control.

II. Concept and Methodology

In AECVT, synthetic capacitance plates are formed by a combination of many small segments. Fig. 1 is an illustration of the adaptive concept built upon on a conventional plate arrangement. Fig. 1(a) shows a typical ECVT sensor with 12 conventional plates whereas Fig. 1(b) and 1(c) depict the capacitance plate used in a conventional sensor deployment and in an adaptive sensor deployment, respectively. In Fig. 2, the whole sensor is comprised by small segments that can be configured and activated to form various plates' shapes and voltage envelopes, respectively. As it will be explained in more detail further below, each segment in the adaptive plate can be activated by voltages of different amplitudes, frequency, and/or phase shifts. The response from all segments of a given synthetic plate are then gathered and represented by an output voltage through a current-to-voltage amplifier. This approach solves the challenge mentioned before, which has persisted since the early days of ECT, centered on the desire for enhancing the resolution by increasing the available number of independent capacitance measurements. Increasing the latter by simply increasing the number of plates through size reduction (without combining individual signals to form synthetic plates) is not feasible because reduces the SNR of each acquired capacitor response. Such capacitance variation measurement in ECT or ECVT is challenging because one it typically confronted with the need to detect capacitance variations in the order of femto-farads in a background of parasitic capacitances that can be up to three orders of magnitude larger.

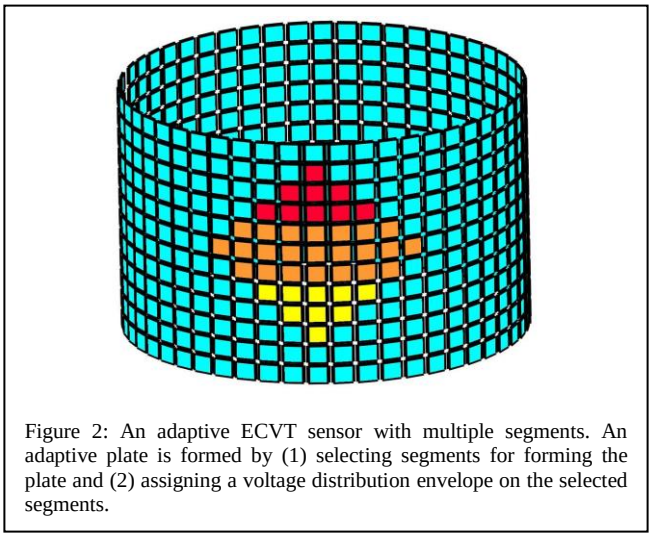

Figure 2: An adaptive ECVT sensor with multiple segments. An adaptive plate is formed by (1) selecting segments for forming the plate and (2) assigning a voltage distribution envelope on the selected segments.

The proposed AECVT enables an increase in the number of independent capacitance measurements by means of a large number of possible synthetic plates, while maintaining the average area of the (synthetic) plates nearly invariant and hence not sacrificing SNR. Synthetic plates also enable a more uniform spreading of the desired sensitivity map across the imaging domain to reduce the ill-posedness of the reconstruction problem. At the same time, they also enable a more flexible control of sensor sensitivity in a certain area of the imaging domain on a reconfigurable fashion, by controlling the charge density distribution on each synthetic plate accordingly.

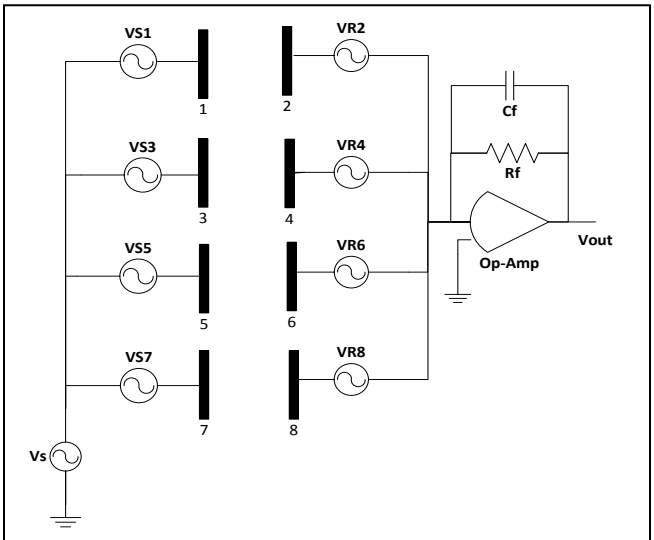

Figure 3: Current-to-voltage amplifier for receiver and sender adaptive plates, each with four segments. The input current to the current-to-voltage amplifier is the sum of the currents from each sender adaptive plate segment to all receiver plate segments.

In Fig. 3, an AECVT sensor circuit with four sender segments and four receiver segments is sketched for illustration. All segments are activated by a main voltage source. The voltage differences across each pair of

sender/receiver segments are then controlled or tuned by intermediate voltage sources before the sending segments and after the receiver segments. This arrangement introduces a current through each pair of sender and receiver segments that depends on the voltage difference as well as the capacitance between them. The operational amplifier in Fig. 3 collects all the currents from the connected segments and transforms them to a voltage that is dependent on the values of the feedback resistor and capacitor. The output voltage can be related directly to an equivalent synthetic plate with a given voltage distribution. The voltage distribution across the synthetic plate can be controlled by changing the amplitude and phase of the intermediate voltages sources on each segment. This voltage distribution is referred to as the "envelope" of the synthetic plate. Envelopes of different frequencies and phases can be introduced to yield synthetic plates with various sensitivity maps. By applying different envelopes, various synthetic plates can be formed providing new independent measurements without the need for any new physical plate.

To illustrate this concept further, the circuit in Fig. 3 is briefly analyzed. To simplify the notation, odd numbers are assigned for sender segments and even numbers for receiver segments. The total current that enters the operational amplifier is the sum of the currents from all segment combinations. For simplicity, we assume that all voltage differences have same phase. Also for simplicity, we assume zero or one level of coupling between capacitor segments. This means that there are two possible paths through which the current can pass from sender to receiver segments: The first path directly from each sender segment to every receiver segment (sender-receiver) and the second path through a first-order coupling between sender segments to all receiver segments (sender-sender-receiver). For the first path, the total current generated in the arrangement of Fig. 3 is:

$$i^{(0)} = \sum_{m=1,3,5,7} \sum_{n=2,4,6,8} \Delta V_{mn} \omega C_{m,n}. \quad (1)$$

Where $i^{(0)}$ is the current generated assuming zero-order coupling between sender segments, ΔV_{mn} is the voltage difference between the m-th sender and n-th receiver pair, respectively. Moreover, ω is the angular frequency of the excitation voltages, and $C_{m,n}$ is the mutual capacitance between the m-th sender and n-th receiver segments. Since ω is assumed the same for all voltage differences, it will be dropped from the following equations by simply setting ω=1. Note that in an AECVT sensor, the product of the voltage difference ΔV_{mn} and capacitance $C_{m,n}$ between each sender and receiver plates is the quantity that actually determines the capacitance representing the contribution of that segment combination (e.g., the synthetic capacitance) to the sensor sensitivity matrix. The current in equation (1) can be decomposed as

$$i^{(0)} = \sum_{m=1,3,4,7} i_m^{(0)} \quad (2)$$

where each term above is the contribution from an individual sender segment under zero-order coupling only, that is:

$$i_m^{(0)} = \sum_{n=2,4,6,8} \Delta V_{mn} C_{m,n} \quad (3)$$

where $i_m^{(0)}$ is simply the current generated from the m-th segment in a zero-order coupling configuration. Another feature that demonstrates flexibility of the present approach is that it is possible to obtain "reversed" virtual capacitances by applying negative voltage differences between plate segments.

We can next examine the first-order coupling. Considering, for example, the interaction between sender plate 1 and sender plate 3, the associated current is

$$i_{13}^{(1)} = \Delta V_{13} C_{13} // i_3^{(0)} - \Delta V_{13} C_{13} // i_1^{(0)} \quad (4)$$

where the // symbol simply denotes the parallel equivalent of the virtual capacitance between both sides of the // symbol. Solving Equation (4) yields:

$$i_{13}^{(1)} = \frac{(\Delta V_{13} C_{13})^2 (i_3^{(0)} - i_1^{(0)})}{(\Delta V_{13} C_{13} + i_3^{(0)})(\Delta V_{13} C_{13} + i_1^{(0)})} \quad (5)$$

which can be rearranged as:

$$i_{13}^{(1)} = \frac{(i_3^{(0)} - i_1^{(0)})}{\frac{(\Delta V_{13} C_{13} + i_3^{(0)})}{(\Delta V_{13} C_{13})} \frac{(\Delta V_{13} C_{13} + i_1^{(0)})}{(\Delta V_{13} C_{13})}} \quad (6)$$

Equation (6) presents the current generated from the first order coupling as a function of the virtual capacitance between sender plates one and three. This equation illustrates that, to reduce the effect of coupling between neighboring sender segments, the virtual capacitance can be minimized by decreasing either the voltage difference or the physical (mutual) capacitance between them.

III. Sensitivity Matrix Results

We should first note that quasi-static field distributions are assumed here (as typical in ECT), i.e. the signal frequency is sufficiently low so that displacement currents can be safely ignored and the electric field distribution inside the imaging domain corresponds to that of a field governed by Poisson equation. This is predicated on the fact that the wavelength of operation is much larger than any of the linear dimensions of the imaging domain. This also means that all field and sensitivity distributions presented here are scale invariant as long as quasi-static conditions are met.

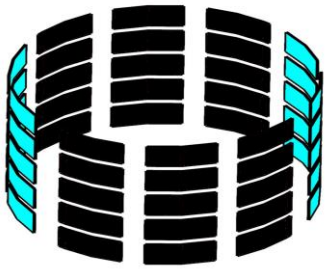

Figure 4: Two opposite synthetic plates (indicated in black), each with 15 segments distributed symmetrically on a 3-by-5 matrix.

The sensitivity matrix of an ECVT sensor is a map of capacitance variations with respect to a set of discrete dielectric perturbations in the imaging domain [15,16] and constitutes the basic input used by image reconstruction algorithms. The sensitivity of an ECVT sensor at a certain location is related to the electric field magnitude squared at that location, which allows for examination of sensitivity maps by solving for the electric field inside the imaging domain.

A cylindrical vessel with circular cross-section, as depicted in Fig. 4, is considered here for simulating sensitivity distributions between two virtual capacitance plates of an AECVT sensor. The vessel has 10 cm diameter. The synthetic plates are opposite to each other and each synthetic plate comprises 15 segments, distributed symmetrically in a 3 × 5 matrix. The height of each segment is 1.5 cm, and each covers 27^0 in azimuth along the column circumference. The distance between adjacent segments is 4 mm along the vertical direction and 8^0 along the azimuth plane.

In the examples that follow, only changes in the excitation voltage amplitude will be discussed for simplicity; in other words, segments in the receiver plate are activated by different voltage amplitudes but same frequency and phase. For the receiver plate, an identical voltage pattern is used.

In Fig. 5, a voltage distribution of 3V on all source segments is employed to mimic a conventional ECVT plate with equipotential surface. In this Figure and all subsequent ones, the voltage impressed on each segment is represented in a matrix format, as shown (note that the small gaps between the segments are not represented). The percentages indicated in the Figure captions refer to the respective vertical heights along the synthetic plates corresponding to the cross-sectional sensitivity distributions plotted. In Fig. 5, regions close to the plate edges yield higher sensitivity due to stronger concentration of electric field lines from the activated segments to the adjacent grounded segments. Higher sensitivity is also visible at the center of the imaging domain.

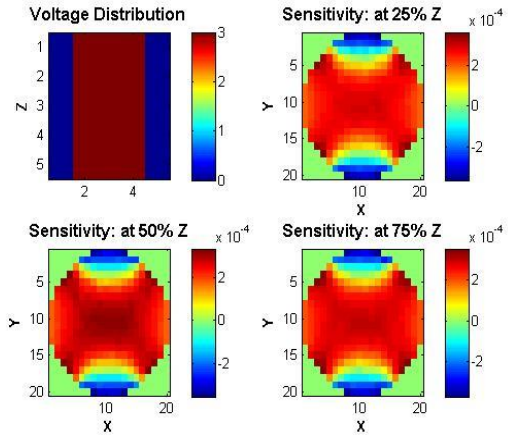

Figure 5: Sensitivity distribution in the column volume and along the height of the sensor at 25% (top-right), 50% (bottom-left), 75% (bottom-right) for the given voltage distribution on synthetic plate segments (top-left).

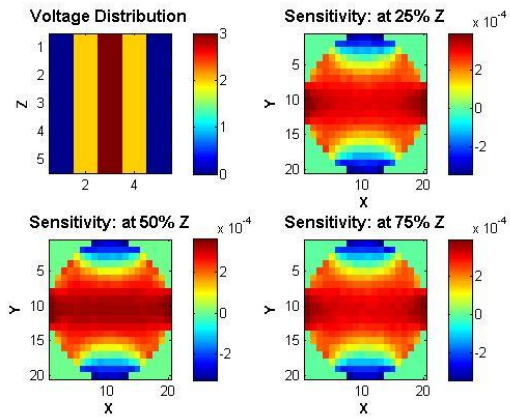

Figure 6: Sensitivity distribution in the column volume and along the height of the sensor at 25% (top-right), 50% (bottom-left), 75% (bottom-right) for the given voltage distribution on synthetic plate segments (top-left).

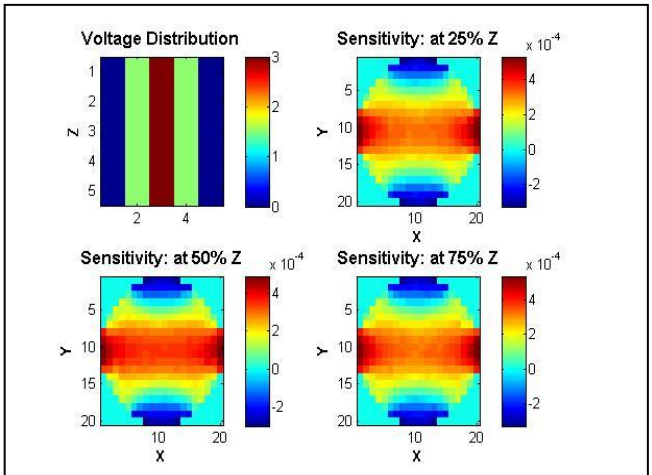

Figure 7: Sensitivity distribution in the column volume and along the height of the sensor at 25% (top-right), 50% (bottom-left), 75% (bottom-right) for the given voltage distribution on synthetic plate segments (top-left).

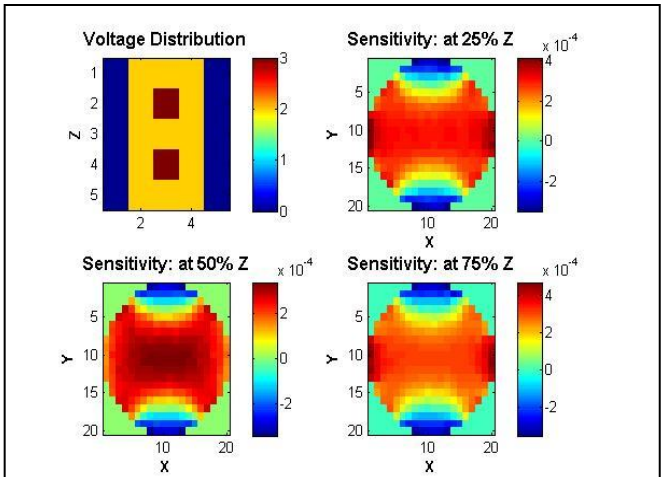

Figure 8: Sensitivity distribution in the column volume and along the height of the sensor at 25% (top-right), 50% (bottom-left), 75% (bottom-right) for the given voltage distribution on synthetic plate segments (top-left).

In order to illustrate the flexibility provided by AECVT, voltage distributions across the same matrix of segments are next changed to manipulate the sensitivity distributions in space. In Fig. 6, the voltage distribution is adjusted to focus the sensitivity of the sensor along a much narrow "corridor" between the synthetic-sender and -receiver plates. This is achieved by tapering the voltage along the transverse direction away from the center of the synthetic plate. In this case, the voltage along the center vertical column is again set to 3V. The next two adjacent vertical rows of segments are set at 2V and all others are grounded. By changing the tapering away from the center row one can further adjust the sensitivity. This is illustrated in Fig. 7, where the voltage in the two rows between the center row and the grounded rows is decreased from 2V to 1.5V. This further reduces the sensitivity outside of the targeted "corridor" region. Note that the use of different excitation voltages across segments does *not* change the mutual capacitances between each segment pairs (as those depend only on the geometry) but only the resulting sensitivity map of each synthetic plate through a change on the spatial charge distribution.

In Fig. 8, the voltage is distributed so as to focus the sensitivity vertically, at the center of the column. This is done by setting higher voltages on two non-adjacent segments. Those segments align the electric field in the imaging domain so that the sensitivity is stronger at the *vertical* center of the column, with some sacrifice on horizontal resolution. The ease of exploiting noncontiguous synthetic plate configurations is another salient feature of AECVT. Indeed, an elementary calculation shows that the electrostatic field magnitude away from two small plates of equal potential and separated by a distance h (along the vertical axis) varies approximately according to $|\overrightarrow{E}| \approx |\eta|/[\eta^2 + \left(\frac{h}{2}\right)^2]^{3/2}$ where η represents the distance away from the plates' plane along the equidistance axis. This function has a maximum at $\eta = h/(2\sqrt{2})$ which means that the region of maximum sensitivity can be adjusted by changing h (comprising a noncontiguous synthetic plate).

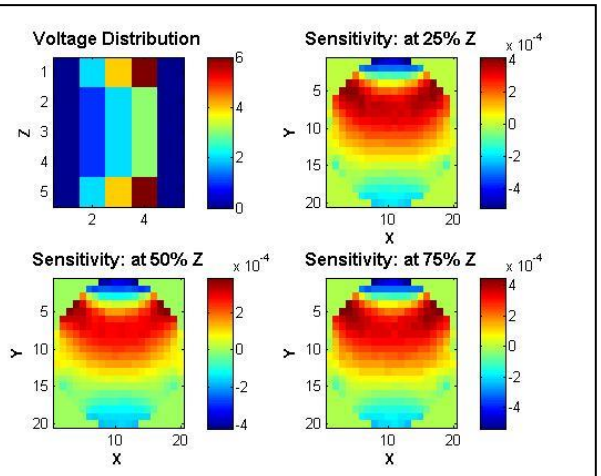

Figure 9: Sensitivity distribution in the column volume and along the height of the sensor at 25% (top-right), 50% (bottom-left), 75% (bottom-right) for the given voltage distribution on synthetic plate segments (top-left).

The higher sensitivity region can also be easily moved to the left or right by adjusting the relative voltages between the sender and receiver synthetic plates. This is illustrated in Fig. 9, where the voltage envelope is focused toward one edge of the adaptive plate, with simultaneous variations along the azimuth and vertical directions. It is evident from this Figure that the distribution of voltages there enhanced the sensitivity toward one side. Note further that introducing a higher voltage level at the top and bottom segments weakened the relative sensitivity around the center of the sensor in the azimuth direction. Closer examination of the sensitivity maps in this case also shows a *negative* sensitivity value at the region adjacent to sensitivity focus and between segments with highest voltages, which can be exploited by image reconstruction algorithms as well. This effect can be reduced or reinforced by tapering the voltage at the edge or increasing its gradient.

For simplicity, 15 segments were used to control the sensitivity distribution in all examples considered here. It is clear that the distribution can be controlled further by using more segments, as implied in Fig. 2.

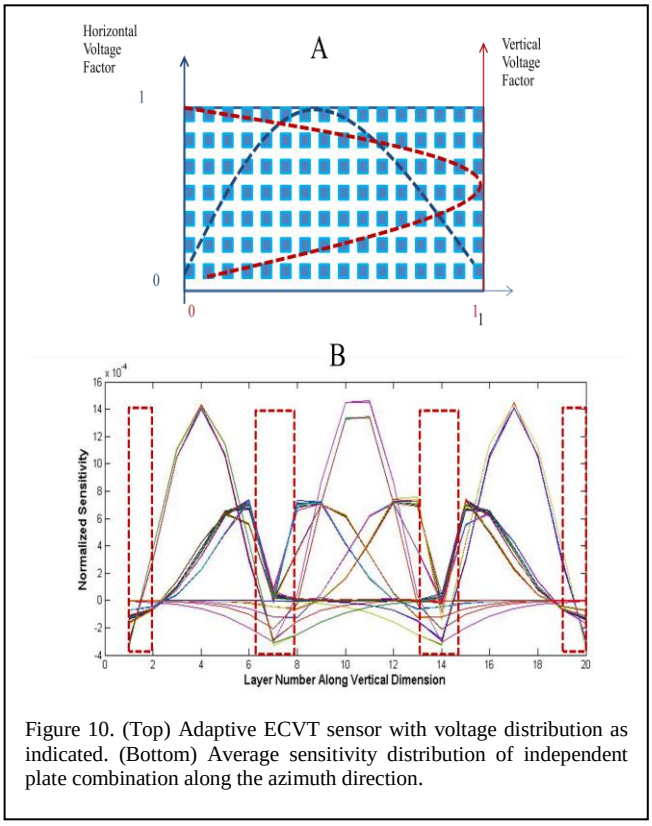

Figure 10. (Top) Adaptive ECVT sensor with voltage distribution as indicated. (Bottom) Average sensitivity distribution of independent plate combination along the azimuth direction.

In Fig. 10, each of the plates in the ECVT sensor of Fig. 1 were replaced with a set of adaptive plates with same overall size (i.e., the case depicted in Fig. 1(c) with a given voltage distribution set across the small segments). The actual voltage distribution impressed over each plate is depicted in Fig. 10(a). In Fig. 10(b), the average sensitivity of all capacitance measurements along the azimuth direction is provided. Since the conventional sensor in Fig. 1 has 12 plates, 66 independent

capacitance measurements are available. For each measurement, the 3D sensitivity map of that plate combination is calculated based on the assigned voltage distribution. This sensitivity distribution is then averaged on each plane, yielding one average sensitivity value per plane along the azimuth direction. Since there are 20 planes assigned for each sensitivity map, Fig. 10(b) depicts 66 curves (one line for each independent capacitance measurement) with 20 points in each curve (number of planes). The red boxes in Fig. 10(b) highlight the "dead zones" where sensitivity is diminished. Dead zones are defined as regions where the sensitivity distributions of *all* capacitance combinations have very low amplitude and/or slope.

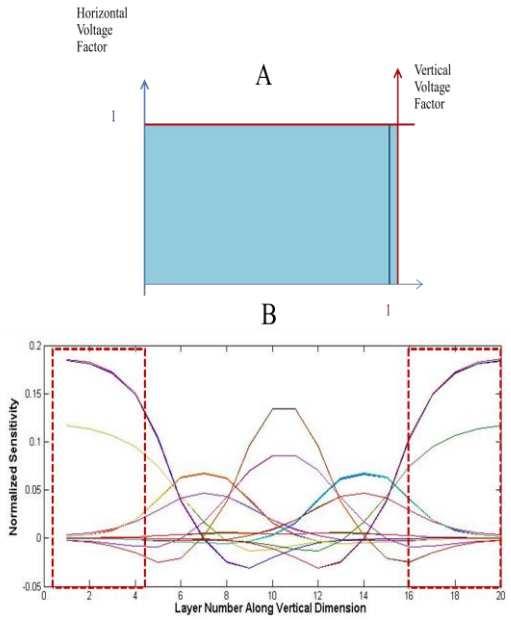

Figure 11: (top) Conventional ECVT sensor with uniform voltage distribution. (bottom) Average sensitivity distribution of independent plate combination along the azimuth direction.

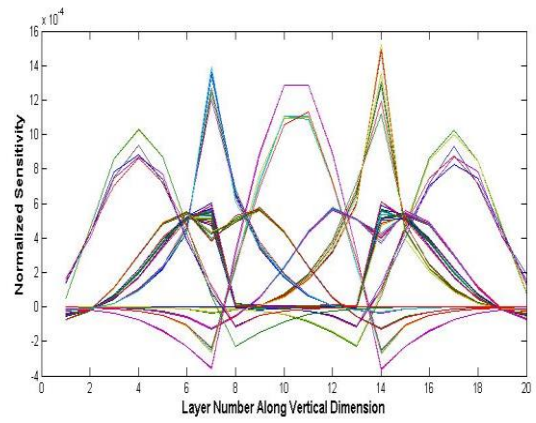

Figure 12: Average sensitivity distribution of independent plate combination along the azimuth direction for a voltage distribution that is a combination of that in Figures 11 and 12.

Similarly, Fig. 11 shows the average sensitivity distribution of a conventional ECVT plate sensor, i.e. with uniform voltage across the plate. In Fig. 11(b), the average sensitivity of all capacitance measurements along the azimuth direction is provided, as done in Fig 10(b). In such conventional plate configuration, "dead zones" are located at the top and bottom of the sensing region.

Next, the direct sum of the voltage distributions used in Figs. 10 and 11 is applied to the adaptive plate as an attempt to eliminate "dead zones". In this case, the voltage distribution in the adaptive plate is set as a half-cosine cycle with a DC shift added to it. This produces the average sensitivity distributions depicted in Fig. 12, where no dead zones are visible. This again shows the flexibility of adaptive sensors in configuring the sensitivity distributions to increase the number of independent acquisitions.

Since the number of possible plate pair combinations enabled by AECVT is greater than in conventional ECVT systems of same size, the acquisition time is expected to increase under otherwise identical conditions. Nevertheless, this increase is only linear versus the overall number of synthetic capacitance pairs employed, and, if necessary, can be compensated by increasing the frequency of operation (as long as quasi-static conditions remain valid). Nevertheless, there are some scenarios where AECVT could potentially provide faster acquisition times, such as those where some prior information is available on the type/size/number of objects to be imaged. In this case, AECVT could enable better dynamic tracking/imaging by using only a (possibly small) subset of sensor segments. In addition, approaches such as the one recently proposed in [17], can also be potentially adapted to synthetic plates and used to strategically reduce the number of acquisitions in AECVT.

IV. CONCLUSION

In this work, the concept of Adaptive Electrical Capacitance Volume Tomography (AECVT) was introduced and illustrated using a number of 3D examples. AECVT is based on the utilization of synthetic capacitance plates, configured by applying excitation voltages with different amplitudes to a number of small individual segments comprising each plate. The segments are connected together through a dedicated circuit to provide an output that mimics that of a capacitance plate with a tailored voltage distribution across it. AECVT provides an enlarged set of virtual (not necessarily contiguous) capacitance plate shapes, while still being able to meet a minimum plate area criterion set by a required SNR. The increased number of capacitance measurements, along with the ability to focus the sensitivity distributions onto desired regions of the imaging domain, provides added flexibility to the imaging reconstruction process in comparison to conventional ECVT. The synthetic plate shapes and sizes can be configured either a priori based on pre-determined imaging requirements (for example, enhanced resolution on particular regions of the domain) or they can be controlled dynamically in a reconfigurable fashion (i.e., "on-the-fly" during the

imaging reconstruction process itself). The study of the performance of reconstruction algorithms exploiting AECVT and such enabled reconfigurability is beyond the scope of this paper and will be the subject of a future work.

REFERENCES

[1] W. Warsito, Q. Marashdeh, and L.S. Fan, "Electrical capacitance volume tomography," *IEEE Sensors*, vol. 7, pp. 525–535, Apr. 2007.
[2] W. Warsito, Q. M. Marashdeh and L.S. Fan, "3D and real-time electrical capacitance volume tomography: Sensor design and image reconstruction," PCT/US2006/010352, Publ. Sep., 28, 2006.
[3] J. Weber and J. Mei, "Bubbling fluidized bed characterization using electrical capacitance volume tomography (ECVT)," *Powder Technology*, vol. 242, pp. 40-50, July 2013.
[4] C. G. Xie et al., "Electrical capacitance tomography for flow imaging: System model for development of image reconstruction algorithms and design of primary sensor," *Proc. Inst. Elect. Eng. G*, vol. 139, pp. 89–98, 1992.
[5] W. Q. Yang and L. Peng, "Image reconstruction algorithms for electrical capacitance tomography," *Meas. Sci. Technol*., vol. 14, no. 1, R1-R13, 2003.
[6] D. Watzenig and C. Fox, "A review of statistical modelling and inference for electrical capacitance tomography," *Meas. Sci. Technol*., vol. 20, 052002, 2009.
[7] F. Wang. Q, Marashdeh, L.-S. Fan, and W. Warsito, "Electrical capacitance volume tomography: Design and applications," *Sensors*, vol. 10, pp. 1890-1917, 2010.
[8] W. C. Chew, *Waves and Fields in Inhomogeneous Media*, Ch. 7, IEEE Press, 1995.
[9] S. Quek, S. Mohr, N. Goddard, P. Fielden and T. York, "Miniature electrical tomography for micro-fluidic systems," *6th World Congress on Industrial Process Tomography*, Beijing, China, 2010.
[10] Q. Marashdeh, W. Warsito, L.-S. Fan, and F. L. Teixeira, "Nonlinear forward problem solution for electrical capacitance tomography using feed forward neural network," *IEEE Sensors J*., vol. 6, no. 2, pp. 441-449, 2006.
[11] Q. Marashdeh, W. Warsito, L.-S. Fan, and F. L. Teixeira "Nonlinear image reconstruction technique for ECT using a combined neural network approach," *Meas. Sci. Technol*., vol. 17, no. 8, pp. 2097-2103, 2006.
[12] Q. Marashdeh, "Development and implementation of 3-D high-speed capacitance tomography for imaging large-scale, cold-flow circulating fluidized bed," U.S. Dept. of Energy Tech. Rep. Contract no. NT0005654, 2013, Tech4Imaging LLC [Online]. Available: http://www.osti.gov/bridge/servlets/purl/1070175/1070175.pdf
[13] Y. Yang and L. Peng, "A configurable electrical capacitance tomography system using a combining electrode strategy," *Meas. Sci. Technol.*, vol. 24, no. 1, pp. 1–11, Jan. 2013.
[14] Q. M. Marashdeh and L.S. Fan, "Adaptive Electrical Capacitance Volume Tomography," U.S. Patent *13/644,973*, Publ. Apr., 4, 2013.
[15] H. Yan, F. Q. Shao, and S. Wang, "Fast calculation of sensitivity distributions in capacitance tomography sensors," *Electron. Lett*., vol. 34, no. 20, pp. 1936–1937, 1998.
[16] Q. Marashdeh and F. L. Teixeira, "Sensitivity matrix calculation for fast electrical capacitance tomography (ECT) of flow systems," *IEEE Trans. Magn*., vol. 40, no. 2, pp. 1204-1207, 2004.
[17] Y. Li and D. J. Holland, ``Fast and robust 3D electrical capacitance tomography,'' *Meas. Sci. Technol.*, vol. 24, 105406, 2013.

Qussai Marashdeh received the B.S. degree in electrical engineering from the University of Jordan, Amman, Jordan, in 2001, and both the M.S. and Ph.D. degrees in electrical engineering while affiliated with the Electroscience Laboratory, The Ohio State University, Columbus, in 2003 and 2006, respectively. He also received the M.S in chemical engineering and the M.B.A. from The Ohio State University in 2009 and 2012, respectively.

He is cofounder, President, and CEO of Tech4Imaging LLC, a Startup Company aimed at advancing capacitance tomography technology and its applications. His research interests include electrical tomography systems, electrostatics, optimization, multi-phase flow, and inverse problems.

Fernando L. Teixeira received the B.S. and M.S. degrees in electrical engineering from the Pontifical Catholic University of Rio de Janeiro, and the Ph.D. degree in electrical engineering from the University of Illinois, Urbana-Champaign. He was a Postdoctoral Associate with the Massachusetts Institute of Technology and since 2000 he has been with The Ohio State University, where he is now a Professor with the Department of Electrical and Computer Engineering and affiliated with the ElectroScience Laboratory.

Dr. Teixeira is a recipient of the NSF CAREER Award, the triennial Booker Fellowship from the International Union of Radio Science, and the Outstanding Young Engineer Award from the IEEE Microwave Society (MTT-S). He currently serves as an Associate Editor for the IEEE ANTENNAS AND WIRELESS PROPAGATION LETTERS. His current research interests include electromagnetic sensors for hydrocarbon exploration, computational electromagnetics, and inverse scattering.

Liang-Shih Fan received the B.S. degree in chemical engineering from National Taiwan University in 1970, the M.S. and Ph.D. degrees in chemical engineering from West Virginia University in 1973 and 1975, respectively, and the M.S. degree in statistics from Kansas State University in 1978. He is Distinguished University Professor and C. John Easton Professor in Engineering in the Department of Chemical and Biomolecular Engineering at Ohio State University.

Professor Fan is a member of U.S. National Academy of Engineering, an Academician of Academia Sinica, and a Foreign Fellow of Chinese Academy of Engineering, Australia Academy of Technology Science and Engineering and Mexican Academy of Sciences. His research interests include fluidization, multiphase flow, particulate reaction engineering, electrical tomography, and energy and environmental systems.